Chinese Journal of
POLYMER SCIENCE

RESEARCH ARTICLE

https://doi.org/10.1007/s10118-023-2972-9
Chinese J. Polym. Sci. **2023**, *41*, 1805–1817

Generation of Tough Poly(glycolic acid) (PGA)/Poly(butylene succinate-*co*-butylene adipate) (PBSA) Films with High Gas Barrier Performance through *In situ* Nanofibrillation of PBSA under an Elongational Flow Field

Fan Yang, Cai-Li Zhang*, Yu Han, Zhi-Rui Ma, and Yun-Xuan Weng

College of Chemistry and Materials Engineering, Beijing Key Laboratory of Quality Evaluation Technology for Hygiene and Safety of Plastics, Beijing Technology and Business University, Beijing 100048, China

Electronic Supplementary Information

Abstract Poly(glycolic acid) (PGA) is derived from glycolide obtained by fermenting pineapples or sugarcane, which has excellent gas barrier properties and a small carbon footprint. PGA is a potential substitute for the current aluminum-plastic composite films used in high barrier packaging applications. However, its poor ductility and narrow processing window limit its application in food packaging. Herein, poly(butylene succinate-*co*-butylene adipate) (PBSA) was used to fabricate PGA/PBSA blend films through an *in situ* fibrillation technique and blown film extrusion. Under the elongational flow field used during the extrusion process, a unique hierarchical structure based on the PBSA nanofibrils and interfacially oriented PGA crystals was obtained. This structure enhances the strength, ductility and gas barrier properties of the PGA/PBSA blend film. In addition, an epoxy chain extender (ADR4468) was used as a compatibilizer to further enhance the interfacial adhesion between PGA and PBSA. 70PGA/0.7ADR exhibited a very low oxygen permeability (2.34×10^{-4} Barrer) with significantly high elongating at break (604.4%), tensile strength (47.4 MPa), and transparency, which were superior to those of petroleum-based polymers. Thus, the 70PGA/0.7ADR blown films could satisfy the requirements for most instant foods such as coffee, peanuts, and fresh meat.

Keywords Poly(butylene succinate-*co*-butylene adipate) (PBSA); Poly(glycolic acid) (PGA); Food packaging films

Citation: Yang, F.; Zhang, C. L.; Han, Y.; Ma, Z. R.; Weng, Y. X. Generation of tough poly(glycolic acid) (PGA)/poly(butylene succinate-*co*-butylene adipate) (PBSA) films with high gas barrier performance through *in situ* nanofibrillation of PBSA under an elongational flow field. *Chinese J. Polym. Sci.* **2023**, *41*, 1805–1817.

INTRODUCTION

Climate change is one of the current major global challenges faced by humanity.[1] To mitigate the effects of climate change and achieve green and sustainable development, carbon neutrality policies have been proposed in China.[2] To complete the carbon cycle, Pujing Chemical Industry Co., Ltd. in China has successfully used carbon monoxide from coal waste gases in the synthesis of poly(glycolic acid) (PGA), which would have otherwise been burnt to carbon dioxide and contributed to greenhouse effects. PGA is a biodegradable polymer that traditionally be synthesized *via* polycondensation of glycolic acid obtained by biosynthetic pathways such as fermentation of recombinant Escherichia coli and microalgae photorespiration. Currently, PGA is used in several applications, such as fracturing balls used for oil and gas extraction as well as surgical sutures because of its high strength and modulus.[3–7] The PGA production capacity in China reached 0.48 million tons in July 2022.[7,8] With the annual increase in the PGA production capacity, there is an urgent need to expand its applications.

The excellent gas barrier properties and mechanical strength of PGA make it an ideal material for packaging. Kureha formed PGA sheets by extrusion, and then biaxially stretched them to produce biaxially oriented flat films for packaging applications.[9] They also investigated the lamination of biaxially oriented PGA films onto other polymer substrates, and the overall performance of the multilayer film was excellent.[10] Despite the excellent strength and modulus of PGA, it is not suitable as a raw material for flexible packaging films because of its low ductility and elongation at break (ε). In addition, there is a relatively small difference between the melting temperature (T_m=222 °C) of PGA and its crystallization temperature (T_c=192–198 °C).[11] In blown film extrusion, the fast crystallization of the material upon cooling of the melt makes it difficult to obtain transparent thin films.[12]

Most recent studies focused on enhancing the ductility of

* Corresponding author, E-mail: zhangcaili@btbu.edu.cn
Received January 27, 2023; Accepted February 22, 2023; Published online April 20, 2023

PGA by blending it with flexible biodegradable polymers such as poly(butylene adipate-*co*-terephthalate) (PBAT),[13–15] polycaprolactone,[16] poly(ethylene glycol-*co*-cyclohexane-1,4-dimethanol terephthalate),[17] and polyethylene oxide.[18] Although the toughness of the blended PGA films was enhanced after the incorporation of these flexible polymers, the barrier properties of the obtained PGA blend films were at least four orders of magnitude lower than that of pristine PGA.[15,19] In addition, these PGA blend films were prepared using the hot-pressing method, which is only suitable for laboratory preparation and not suitable for large-scale applications.

Recently, Wan *et al*. prepared PGA/PBAT (20/80) films using a continuous blown film extrusion process.[20] The oxygen barrier performance of the modified PGA film was three orders of magnitude lower than that of pristine PGA. This is mainly because it is difficult to significantly improve the gas barrier properties of the blend films with low contents of PGA. Our recent work reported a PGA/PBAT blown film with a PGA content of up to 60%, which exhibited a gas barrier performance that is two orders of magnitude lower than that of pristine PGA.[21] This can be attributed to the dispersion of the relatively large size of the PBAT phase and the poor interfacial adhesion between the PGA matrix and PBAT droplets, resulting in a low gas barrier performance of the PGA/PBAT (60/40) films.

In situ fibrillation is an effective method to reduce the dispersed phase size and increase the interfacial adhesion between the two phases. Zhou *et al*.[22] successfully used *in situ* fibrillation to prepare poly(lactic acid) (PLA)/PBAT films. The PBAT nanofibrils retarded the gas diffusion, improved the barrier properties of the PLA/PBAT film, and promoted the PLA oriented crystallization. Whether the dispersed phase can generate fibrils *in situ* depends on two factors: (1) the rheological properties of the molten component (*i.e.*, viscosity and elastic ratio) of the dispersed phase and the interfacial interactions between the matrix components,[23,24] which control the transition of the dispersed phase from droplets to fibers under external tension; and (2) the stability of the fiber structure during the film formation, which is significantly affected by the relaxation and decomposition dynamics of the fibril components. Therefore, under specific processing conditions, which satisfy the required rheological and thermal conditions, fibrils will form in the melt.[25] The addition of the chain extender can also reduce the size of the dispersed phase and strengthens the adhesion of the two phases. Ojijo *et al*.[26] added a multifunctional reactive oligomer ADR to a PLA/poly(butylene succinate-*co*-butylene adipate) (PBSA) blend, resulting in a drastic reduction of the dispersed phase size and an increase the viscosities of the blends. And Sun *et al*.[27] successfully improved the compatibility of PLA/poly(propylene carbonate) films by ADR. In addition, the mechanical properties of the PLA/PBAT/ADR blends prepared by Li *et al*.[28] were superior to those of the blends without the addition of ADR.

PBSA exhibits better ductility and ε than PBAT because its molecular structure does not contain rigid benzene rings, and its mechanical properties are comparable to the widely used low-density polyethylene (LDPE).[29–32] Yousfi *et al*.[33] manufactured poly(isosorbide carbonate-*co*-cyclohexanedimethanol) (PIC)/PBSA films by melt extrusion casting using *in situ* nanofibrillation. Results show that the ε of the blend increased by approximately 670% compared to that of the pristine PIC without sacrificing the tensile strength (σ).

In this study, PBSA was used to fabricate PGA/PBSA blend films *via in situ* fibrillation. Under the elongational flow field used during the blown film extrusion process, the PBSA structure was transformed from droplet-like to nanofibrillar, which can improve the dispersion of PBSA and reduce its size to enhance the gas barrier properties. Moreover, high PGA content (up to 70 wt%) was incorporated in the blown films. To the best of the authors' knowledge, there are no reports on the preparation of high-content blend PGA films using blown film extrusion. Moreover, the crystallization temperature of PGA could be regulated after the addition of PBSA. This can extend the processing window and enable better control of the crystallization stage of the PGA blend films, which significantly help regulate the morphology and transparency of the films and improve their mechanical and gas barrier properties.

EXPERIMENTAL

Materials

PBSA (Japan, molecular weight (Mw)=190 kg/mol, density=1.24 g/cm^3, and glass transition temperature=−43.8 °C was provided by Showa Denko. PGA (Mw=150 kg/mol) was supplied by Pujing Chemical Industry Co., Ltd. (Shanghai, China). A styrene–glycidyl methacrylate oligomer (Joncryl ADR 4468, epoxy equivalent weight=285 g/mol, weight-average molecular weight=7250 kg/mol), which was used as a chain extender, was acquired from BASF (Germany). Dichloromethane was obtained from Honeywell Trading Co., Ltd. (Shanghai, China).

Preparation of Blend Pellets

PGA and PBSA were dried under vacuum at 80 °C for at least 12 h before use. The formulations of PGA/PBSA composites in this work are listed in Table 1. The PGA/PBSA/ADR blend pellets were prepared using a counter-rotating twin-screw extruder (screw diameter=20 mm, and length=40 cm, Rebateco Company, LTE20-40). The extrusion was conducted at a screw speed of 100 r/min and extrusion temperatures of 170–200 °C from the first zone to the die.

Hot-Pressed Films

The extruded pellets were compression molded using a hot-pressing machine (Dongguan Zhenggong Electromechanical Equipment Technology Co., Ltd., China, ZG-20T) to obtain hot-pressed films at a molding temperature of 230 °C under a pressure of 240 kg/cm^2 for 300 s. The samples were then

Table 1 The formulations of this work.

Samples	PGA (wt%)	PBSA (wt%)	ADR (phr)
PBSA	0	100	/
PGA	100	0	/
70PGA	70	30	/
70PGA/0.3ADR	70	30	0.3
70PGA/0.5ADR	70	30	0.5
70PGA/0.7ADR	70	30	0.7

https://doi.org/10.1007/s10118-023-2972-9

naturally cooled at room temperature to obtain the final films.

Blown Films

The blown films were prepared using a single screw extruder (screw diameter = 25 mm and length=30 cm, Kechuang, China, LSJ20). The blown film extrusion was performed at 185 °C–189 °C–189 °C–189 °C from the first zone to the die at a screw speed of 50 r/min and a blow-up speed of 2 m/min. Films with a thickness of 35–45 μm were obtained.

Characterizations

Fourier transform infrared (FTIR) spectroscopy

FTIR spectroscopy was conducted on a PerkinElmer 782 combined with an attenuated total reflection (ATR). 64 Scans were accumulated in the spectral region of 390–4000 cm^{-1} with a spectral resolution of 4 cm^{-1}.

Morphology

The films were cryo-fractured in liquid nitrogen, and their cross-sections were observed using scanning electron microscopy (SEM). To study the two-phase morphology, the films were etched with dichloromethane for 30 min to remove the PBSA phase. To clarify the crystalline morphology of PGA, the PBSA and amorphous PGA were etched using a mixture solution of sodium hydroxide (0.05 mol/L) and water-methanol (1:1, *V*:*V*) at 25 °C for 24 h. Next, a field emission SEM (FEI, Quanta 250 FEG, USA) with an accelerating voltage of 10 kV was used to observe the samples, which were gold-coated for 2 min before the scanning process. Quantitative analysis of the diameter distribution of PBSA nanofibrils was carried out by Image-Pro Plus 6.0 image analysis system and Origin 2018 software.

Rheology properties

Rheological measurements were conducted at 233 °C under the oscillation mode using an Anton Paar MCR-502 rotational rheometer equipped with two parallel plates (spacing=1 mm and diameter=25 mm). The frequency range was 0.1–100 rad/s and maintained a low strain amplitude of 0.1%.

Differential scanning calorimetry (DSC)

The crystallization behavior of samples was characterized using a DSC (TA2500, USA). Under nitrogen environment, a sample (5–6 mg) was heated from 20 °C to 250 °C at a rate of 20 °C/min. The degree of crystallinity (χ_c) was calculated according to Eq. (1):

$$\chi_c = \frac{\Delta H_m - \Delta H_{cc}}{w\%\Delta H_m^0} \times 100\% \quad (1)$$

where ΔH_m is the enthalpy of melting for PGA, ΔH_{cc} is the enthalpy of cold crystallization, ΔH_m^0 is the melting enthalpy of 100% crystalline PGA homopolymers (ΔH_m^0=183.2 J/g),[34] and *w*% is the weight fraction of the PGA component in the samples.

Wide-angle X-ray diffractograms (WAXD) and small-angle X-ray scattering (SAXS)

WAXD patterns were recorded using a Bruker D8 advanced X-ray diffractometer with Cu K*α* radiation (*λ*=1.54 Å, 40 kV, 40 mA). The samples were scanned from 3° to 40° at a scan rate of 3 (°)/min. The relative crystallinity (X_c) of the blend films was determined by the MDI Jade 6 software (Materials Data Inc., USA) using Eq. (2):

$$X_c = \frac{I_a}{I_c + I_a} \times 100\% \quad (2)$$

where I_c is the diffraction integral intensity of the crystalline part and I_a is the scattering integral intensity of the amorphous part.

SAXS analysis was carried out using an Xenocs Xeuss 3.0 SAXS device at 50 kV and 600 μA with Cu K*α* radiation (1.54 Å) at a sample-to-detector distance of 800 mm. The long period (*L*) of the crystalline layer combined with one interlamellar amorphous layer was calculated according to Bragg's law ($L = 2\pi/q_{max}$, where q_{max} is the peak of the scattering vector, *q*, in the SAXS one-dimensional curve). The crystal layer thickness, d_c, (Å) and the amorphous layer thickness, d_a, (Å) were calculated by the following equations: $d_c = L \times X_{c\text{-}PGA}$ and $d_a = L - d_c$, respectively. The $X_{c\text{-}PGA}$ was obtained based on the first heating scan in the DSC curves of the blown and pressed films.

Pole figure

The pole figures of the samples were obtained using a Schulz back reflection method on an X-ray diffractometer (Panalytic Xpert MRD, Cu target voltage=40 kV, current=40 mA). Three incomplete pole figures (0°≤*α*≤70°, 0°≤*β*≤360°) were obtained for each diffraction plane, *i.e.*, (110) and (020) for PGA (diffraction angles, 2*θ*=22.06° and 28.7°, respectively). The pole figure of (002) was developed based on the orientation distribution function (ODF) by MulTex software.

Transmittance

UV-Vis transmittance spectrum of the films within the 200–800 nm range was acquired by a UV-3600 UV-Vis spectrophotometer (Shimadzu, Japan).

Oxygen transport properties

The O_2 permeability (*P*) of the PGA/PBSA film (area=10 cm^2) was tested according to the ASTM D3985 standard using an oxygen permeability tester (VAC-V1, Jinan Languang Electromechanical Technology Co., Ltd.) at a temperature of 23 °C and relative humidity (RH) of 30%. Each test was performed three times and the average value was calculated.

The relationship between the diffusion coefficient (*D*) and the solubility coefficient (*S*) is given in Eq. (3):

$$P = D \times S \quad (3)$$

where *P* is the permeability in barrer (1 Barrer = 1×10^{-10} cm^3_{STP}·cm/cm^2·s·cmHg). Diffusion coefficients were calculated based on the permeation experiments using the time-lag method as shown in Eq. (4):

$$D = \frac{l^2}{6\theta} \quad (4)$$

where *D* is the diffusion coefficient (cm^2/s), *l* is the film thickness, and *θ* is the time lag. The sorption-diffusion model ($S = P/D$) was used to back-calculate *S* (cm^3_{STP}·cm^{-3}·$cmHg^{-1}$).

Water vapor transport properties

The water vapor permeability (WVP, 10^{-14} g·cm/cm^2·s·Pa) and water vapor transmission rate (WVTR, g·m^{-2}·day^{-1}) were tested by a C360M water vapor permeameter following the GB/T 1037-2021 standard (at 38 °C, RH=90%). Three replicates were obtained for each component.

Mechanical properties

The mechanical properties of the PGA/PBSA films were obtained based on the ASTM D638 standard using a CMT6104 electronic universal testing machine with a load cell of 50 N and a crosshead speed of 100 mm/min in the machine direction (MD)

https://doi.org/10.1007/s10118-023-2972-9

and in the transverse direction (TD) of the films. The tearing strength of the trouser-shaped specimens was measured according to the ASTM D1938-19 standard at speeds of 10 and 5 mm/min in the MD and TD of the films, respectively. Each sample was conditioned at 25 °C and a RH of 50% for at least 72 h before the test. A minimum of five replicates were conducted for each sample under the same conditions.

RESULTS AND DISCUSSION

The combined action of applying an external stress field and using a chain extender can significantly change several morphological characteristics, such as crystallinity, orientation, and phase separation behavior, of the PGA/PBSA films, resulting in significant variations in their hierarchical structure. Thus, the effects of the external stress field and chain extender content on reeducation the structure and properties of the prepared PGA/PBSA composite films were discussed and compared in detail.

FTIR Analysis

To identify the interactions between the polymer molecular chains, FTIR measurements were performed on the neat polymers, blends, and chain extender. When the chain extender reacts with the carboxyl groups of PGA and PBSA, respectively, the epoxy group of ADR is destroyed and its characteristic bands at 843 and 907 cm^{-1} disappear. The disappearance of these two characteristic peaks in the spectrum of the 70PGA/0.5AD sample (Fig. S1 in the electronic supplementary information, ESI) is attributed to the ring-opening reaction of the epoxy group of ADR with the carboxyl end groups of PGA and PBSA. Scheme 1 shows the schematic of the reaction mechanism of ADR with PGA and PBSA.

Phase Morphologies of the PGA/PBSA Composite Films

The phase morphology of the PGA/PBSA composite films is the main factor affecting their barrier and mechanical properties. Fig. 1 shows the phase morphology of the cryo-fractured PGA/PBSA blown films along the MD. It was difficult to distinguish between the PBSA phase and the PGA matrix after the incorporation of the ADR chain extender because of the improved interfacial interaction.

Because the solubility parameters of PGA and PBSA are quite different, the dispersed PBSA phase can be exclusively etched using dichloromethane. Fig. 2 shows the phase morphology of the cryo-fractured surfaces of the PGA/PBSA blown films along the MD and TD after the etching of the PBSA phase. Figs. 2(a)–2(d) indicate the *in situ* conversion of the dispersed phase of PBSA into nanofibrils along the MD under the effect of the intensively elongational flow field. This is significantly different from the sea-island distribution of PBSA in the pressed films (Fig. S2 in ESI).

Moreover, the diameter of the PBSA nanofibrillar in the skin layer was smaller than that in the core region. This phenomenon can be ascribed to the gradient in the shear force and cooling rate, resulting in the formation of fibrillar PBSA particles with small diameters in the skin layer under relative

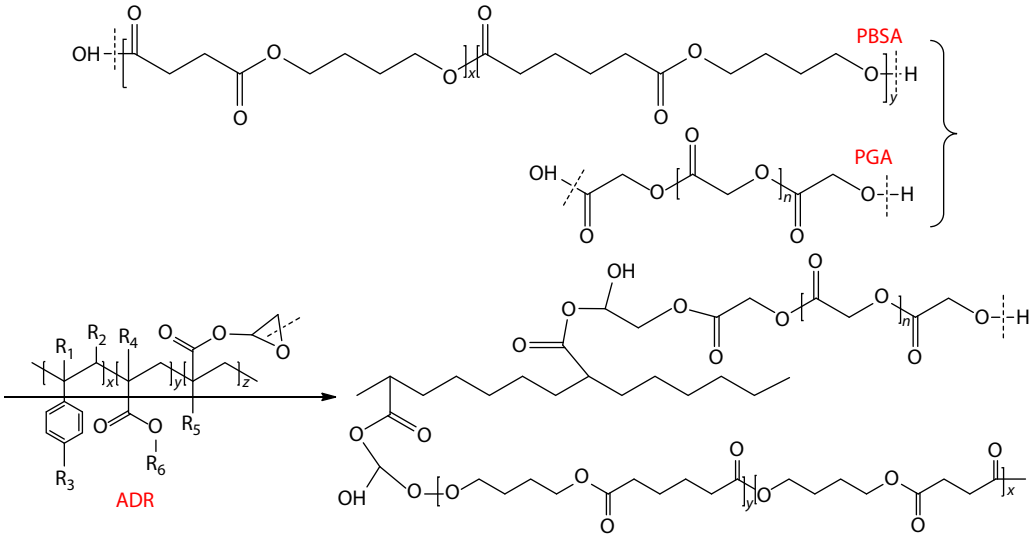

Scheme 1 Schematic of the reaction mechanism of ADR with PGA and PBSA.

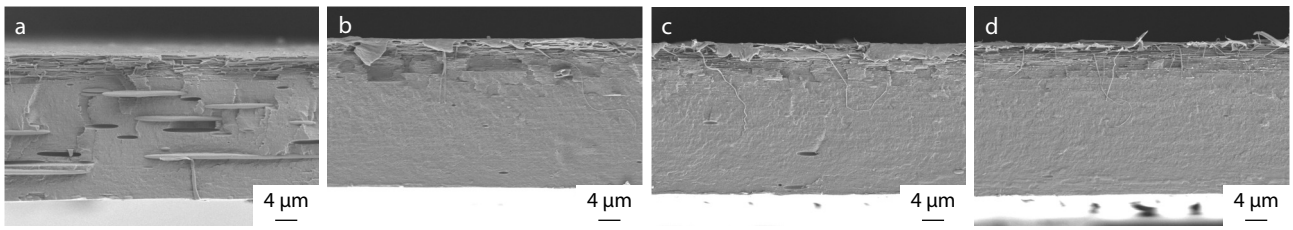

Fig. 1 SEM images of the cryogenically fractured surface along the MD of the 70PGA/ADR blown films: (a) 70PGA, (b) 70PGA/0.3ADR, (c) 70PGA/0.5ADR, and (d) 70PGA/0.7ADR.

https://doi.org/10.1007/s10118-023-2972-9

strong elongational flow field.[35,36] In addition, the content of the chain extender affects the length and diameter of the PBSA fibrils. Thus, the diameter of the nanofibrils decreases with the increase in the content of the chain extender, and the diameter of the nanofibrils decreased from 461.9 nm (no ADR, 70PGA) to 164.4 nm with the addition an ADR amount of 0.7 phr. This confirms that ADR successfully acts as a bridge during the reaction with PGA and PBSA. Thus, the outer layer of the PBSA fibrils is connected to PGA and cannot be etched by dichloromethane, confirming their improved compatibility.[37]

Rheological Properties

The molecular chain entanglement and two-phase interactions can also be characterized based on the rheology properties.

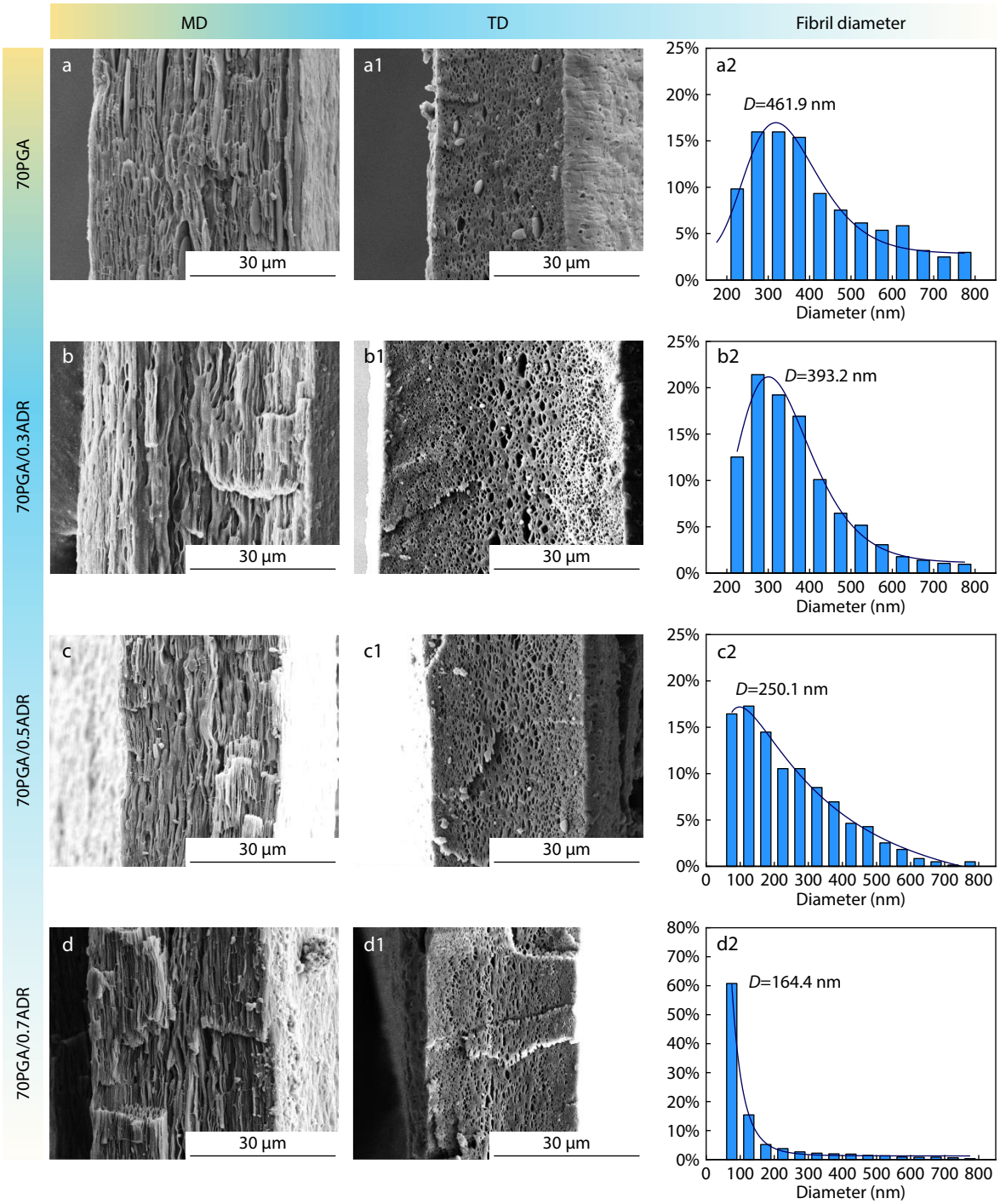

Fig. 2 SEM micrographs of the etched cryogenically fractured surface along the MD of the blown films: (a) 70PGA, (b) 70PGA/0.3ADR, (c) 70PGA/0.5ADR, and (d) 70PGA/0.7ADR; (a1–d1) the corresponding SEM micrographs of the etched cryogenically fractured surface along the TD of the blown films; and (a2–d2) diameter distribution of the PBSA nanofibrils in the blown films.

https://doi.org/10.1007/s10118-023-2972-9

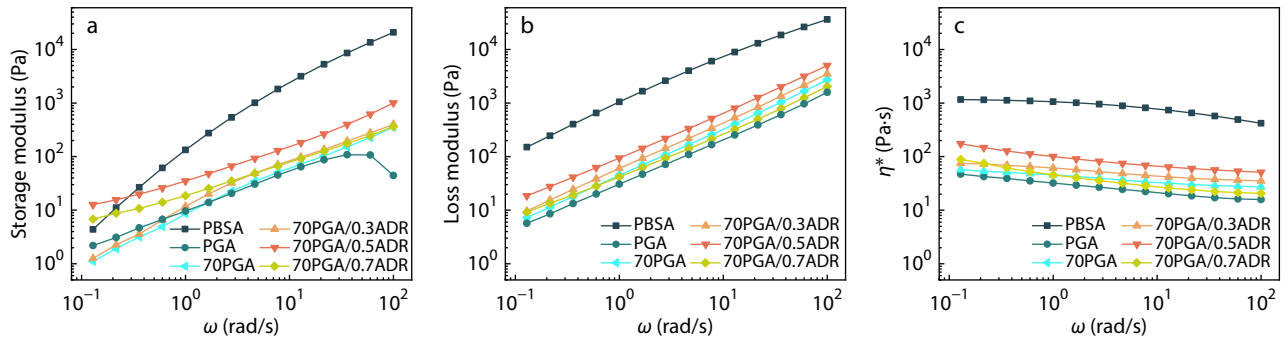

Fig. 3 The dependance of the (a) storage modulus, (b) loss modulus, and (c) complex viscosities (η^*) of the 70PGA blends, neat PGA, and neat PBSA on the shearing frequency.

Fig. 3 shows the dependence of the storage modulus (G'), loss modulus (G''), and complex viscosities (η^*) of neat PGA, PBSA, and their blends on the shearing frequency. PBSA is obtained by the copolymerization of succinic acid, butanediol, and adipic acid, which contains flexible adipic butylene chains in the molecular chain, resulting in the irregularity and flexibility of the molecular chain. Compared to PGA, PBSA has more flexible molecular chains and can be more easily enlarged. PBSA shows much higher G', G'', and η^* than PGA. Compared to PGA/PBSA, after the ADR addition into the blends, these three values first increased then decreased. Moreover, 70PGA/0.5ADR shows the highest values among all blends containing ADR. This indicates that the most entangled structures form in 70PGA/0.5ADR. These results suggest that the addition of ADR causes a chain extension or a branching reaction and further enlarges the structure of the PGA/PBSA blends.[38–40] However, at ADR=0.7 phr, G' and η^* slightly decreased. This may be due to the lubrication and plasticizing effects of some unreacted ADR in the melt structure.[21]

Crystalline Structures and Orientation

DSC was used to study the crystal growth of the PGA crystals, which is induced by the external stress field during the blowing and hot-pressing processes. The DSC second heating scan curves of neat PBSA and PGA are shown in Fig. S3 (in ESI). Fig. 4 shows the resultant DSC first heating curves for the blown and pressed composite films. The peak at 45°C in Fig. 4(a) is attributed to the glass transition (T_g) of the PGA, the cold crystallization peak at 80 °C is attributed to the incomplete crystallization of the PGA in the films, and the peak at 221 °C is the melting peak (T_m) of the PGA in the blended films.

In contrast to the blown films, the heating curve of the hot-pressed films shows no cold crystallization peak (Fig. 4b), indicating that the hot-pressing process enhances the PGA crystals. The information listed in Table 2 indicates that the crystallinity, $X_{c\text{-}DSC}$ of the blown films are lower than that of the pressed films. This can be attributed to the fact that there is a small difference between the T_m (221 °C) and crystallization temperature (T_c=183 °C, Fig. S4 in ESI) of PGA. This makes it difficult to achieve complete crystallization during the rapid cooling in the blowing process. Thus, a cold crystallization occurs at 80 °C during the heating process. Furthermore, the addition of ADR (0.7 phr) increases the peak temperature of the cold crystallization by approximately 3 °C. In addition, the crystallinity also decreases with the increase in the ADR content, indicating that the molecular chain entanglement increases as a result of the chain extension reaction, which hinders the crystal growth.

Typically, the small difference between T_m and T_c will accelerate the crystallization after the cooling of the melt, and makes it difficult to obtain PGA products with amorphous structures.[41] Therefore, it is very difficult to obtain a transparent PGA film. In this study, the crystallization temperature of PGA can be effectively reduced (175–177 °C, Fig. S4 in ESI) by the addition of PBSA, which enables the preparation of transparent extruded films.

The crystalline morphology and macrostructure of the blown and pressed films were further characterized by WAXD

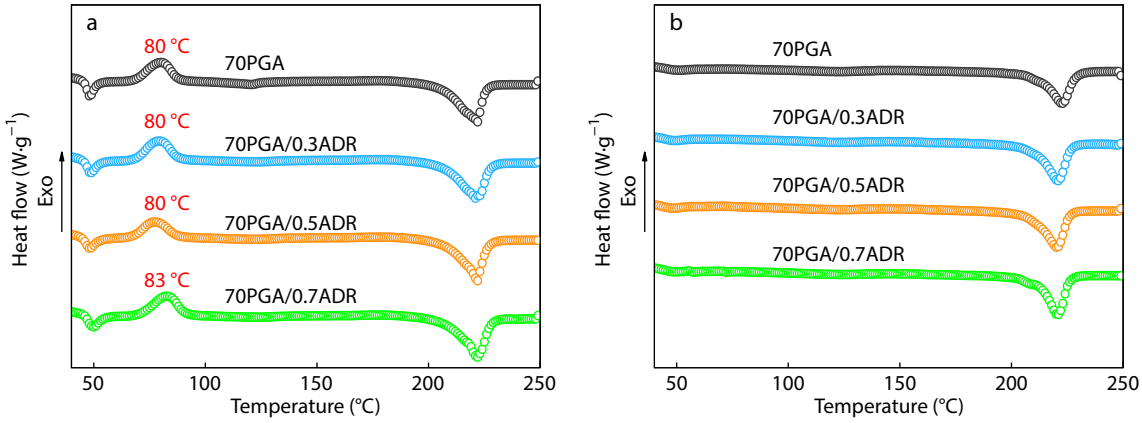

Fig. 4 DSC curves of the first heating scans for the 70PGA/ADR (a) blown films and (b) pressed films.

https://doi.org/10.1007/s10118-023-2972-9

Table 2 Structural parameters of the 70PGA/ADR blown films and pressed films.

	Sample	q_{max} (Å^{-1})	$X_{c\text{-}DSC}$ (%)	$X_{c\text{-}WAXD}$ (%)	L (Å)	d_c (Å)	d_a (Å)
Blown films	70PGA	0.045	18.56	7.39	139.80	25.95	113.85
	70PGA/0.3ADR	0.051	18.11	0.19	123.98	22.45	101.52
	70PGA/0.5ADR	0.057	17.76	1.29	110.62	19.65	90.97
	70PGA/0.7ADR	0.051	15.68	5.37	122.13	19.15	102.98
Pressed films	70PGA	0.052	35.31	34.64	121.20	42.80	78.40
	70PGA/0.3ADR	0.052	34.44	34.16	120.30	41.43	78.87
	70PGA/0.5ADR	0.051	31.89	29.1	124.00	39.54	84.46
	70PGA/0.7ADR	0.052	30.93	27.14	120.30	37.21	83.09

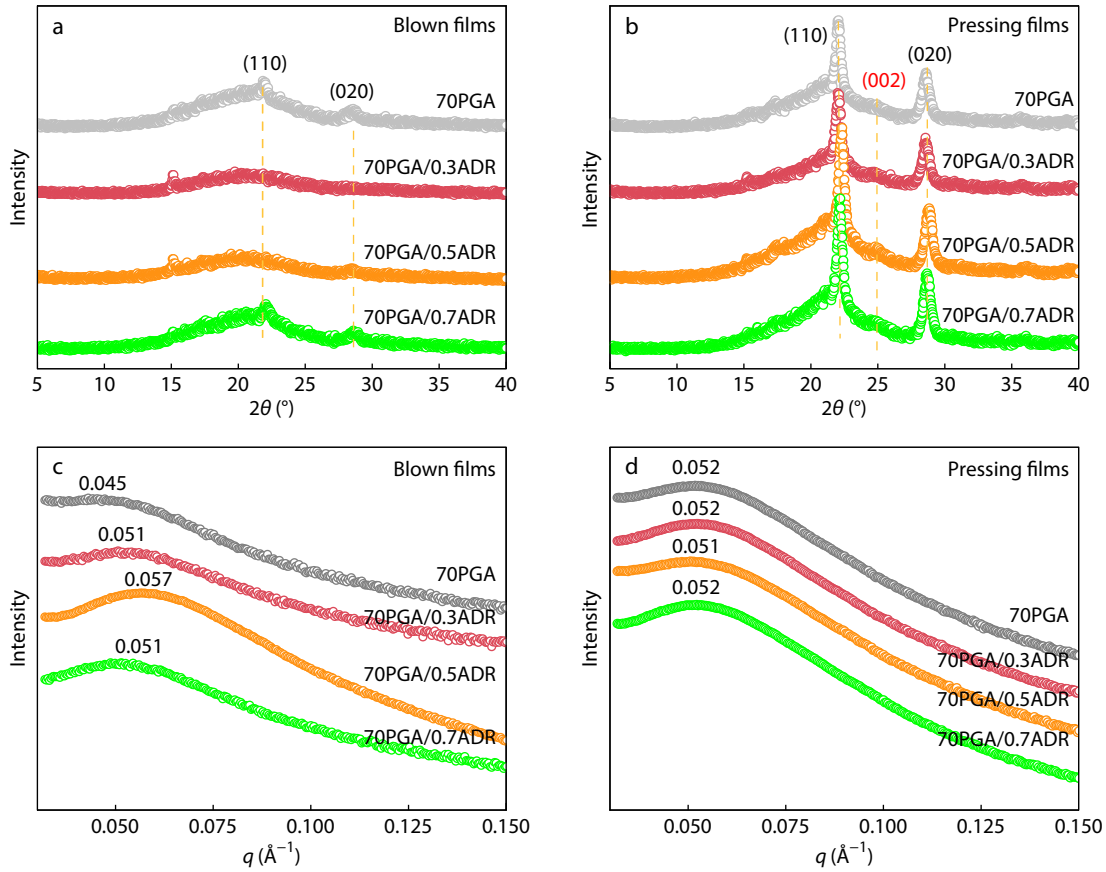

Fig. 5 (a, b) WAXD and (c, d) SAXS patterns of the blown and pressed films.

(Figs. 5a and 5b) and SAXS (Figs. 5c and 5d). Comparing Fig. 5(a) and Fig. 5(b), the intensity of the crystallization peak of the pressed films is clearly higher than that of the blown films, indicating the higher crystallinity of the former. The crystallinity ($X_{c\text{-}WAXD}$) was calculated based on the WAXD profile based on the fitted areas of the amorphous and crystalline phases (Table 2). The crystallinity of the blown film calculated based on DSC is different to that calculated based on WAXD, which is mainly due to the different testing methods. In addition, the (002) planes of PGA disappeared in the WAXD of the blown film. The fact that the (002) plane of PGA can only be detected on the transverse X-ray diffraction profile[42,43] suggests that the blown film has a higher crystal orientation than the pressed films.

To quantitatively evaluate the size of the crystalline superstructure, the SAXS intensity distributions of the blown and pressed films were performed. Figs. 5(c) and 5(d) show the q_{max} value of the peak, which can be used to calculate the long period (L) according to Bragg's law. The crystal layer thickness, d_c, was obtained by $X_{c\text{-}DSC}$ of the blown and pressed films. The amorphous layer thickness, d_a, can be calculated by $d_a = L - d_c$. Table 2 summarizes the obtained q_{max}, L, d_c, and d_a values. Thus, the crystal size of the blown films is lower than that of the pressed films. Therefore, the crystallinity and crystal size of the blown films were lower than those of the pressed films, which can be attributed to the rapid cooling and tensile effect of the flow field during the blowing process.

The molecular orientation of the composite films was also studied using 2D-SAXS (Fig. 6). The 2D-SAXS patterns indicate that the scattering ring of the pressed film is circular, showing an isotropic crystal distribution. The scattering rings of the blown films are elongated along the meridional direction, demonstrating the presence of oriented crystals. To further study the molecular orientation of the blown and

https://doi.org/10.1007/s10118-023-2972-9

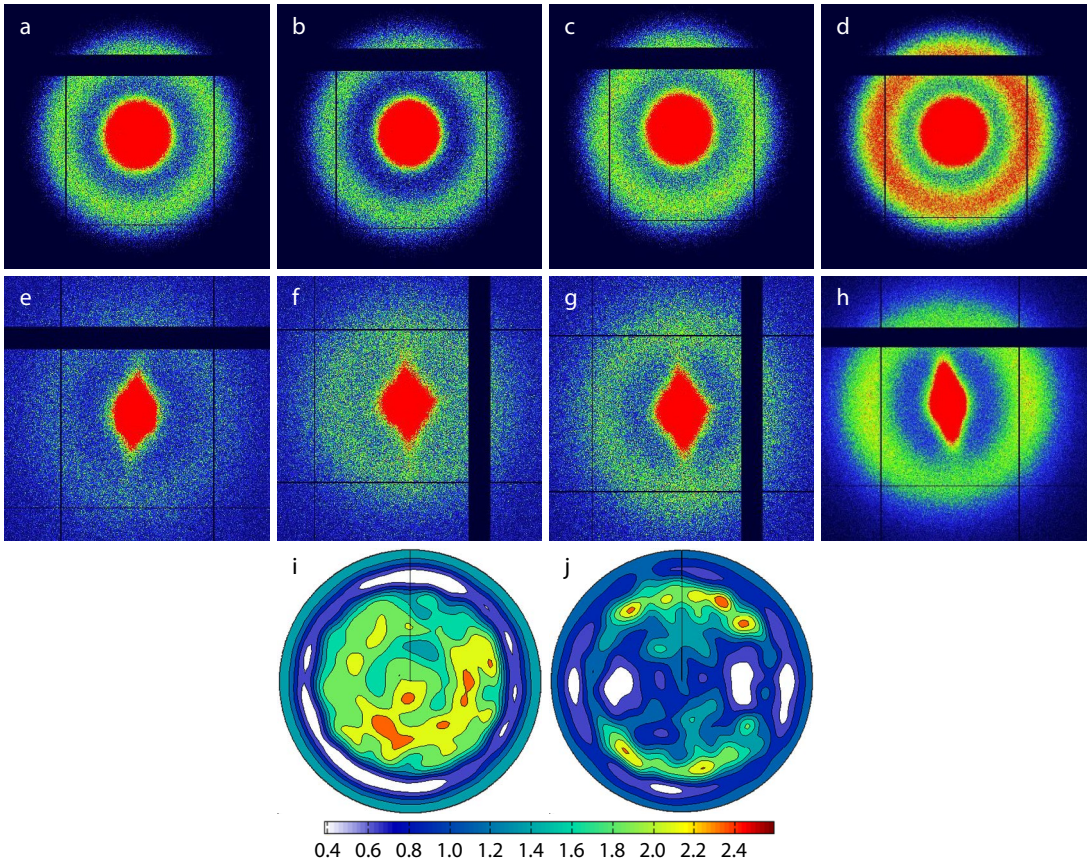

Fig. 6 2D-SAXS patterns of the pressed films: (a) 70PGA, (b) 70PGA/0.3ADR, (c) 70PGA/0.5ADR, and (d) 70PGA/0.7ADR; as well as those of the blown films: (e) 70PGA, (f) 70PGA/0.3ADR, (g) 70PGA/0.5ADR, and (h) 70PGA/0.7ADR. X-ray pole figures of the (002) planes of the PGA crystals in the (i) pressed and (j) blown 70PGA/0.5ADR of films.

pressed films, X-ray pole figures were developed for the (002) planes. The (002) pole figures show the orientation distribution of the *c* axis.[43] Fig. 6(j) indicates that the crystal chain axis (*c* axis) of the blown film is extended in the MD direction.

To characterize the crystalline orientation of PGA, the PGA amorphous phase removed by etching was examined using high-resolution SEM (Fig. 7). Only a slight hydrolysis of PBSA occurs under the alkaline environment during the etching process, and PGA shows faster hydrolysis than PBSA. As shown by the arrows in Figs. 7(a) and 7(b), the hybrid shish-kebab crystals of PGA were arranged on the elongated PBSA fibrils.

Transparency is an important parameter for films used in practical packaging applications. The transmittance of the PGA/PBSA composite films prepared by two different methods were investigated. Fig. 8 indicates that the PGA/PBSA blown films have good optical transmittance in the visible region. In constant, the pressed films show low transmittance. The transparency of plastic is related to its crystal size. The transparency of blends is also related to the size of the dispersed phase, refractive index, and interfacial adhesion between the two phases.[12] In this study, the high transparency of the PGA/PBSA blown films can be mainly attributed to: (1) the low crystallinity and small crystal size of PGA, which enables the visible light to pass through the PGA phase without scattering; and (2) the dispersion of PBSA in the PGA matrix as nanoscale fibrils and the strong interfacial adhesion between PGA and PBSA, which result in weak light scattering at the interface between the two phases. Thus, the PGA/PBSA blown films are highly transparent.

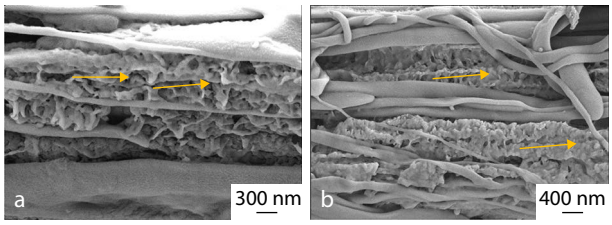

Fig. 7 SEM images of the NaOH-etched (a) 70PGA and (b) 70PGA/0.5ADR blown films.

Barrier Properties

The effect of the processing technology and ADR content on the oxygen permeability (P_{O_2}) of the PGA/PBSA composite films is illustrated in Fig. 9(a). The P_{O_2} of the blown films shows a reduction that is almost two orders of magnitude that of the pressed film. In particular, the 70PGA/0.7ADR blown film exhibits a low oxygen permeability (2.34×10^{-4} Barrer). This is mainly caused by two reasons. (1) Although the crystallinity of PGA in the hot-pressed film is high, the effect of prolonging the gas diffusion path is not clear because of the isotropy and random arrangement of the crystals. (2) PBSA is dispersed in tens of microns in the hot-pressed film. Because the P_{O_2} of PBSA

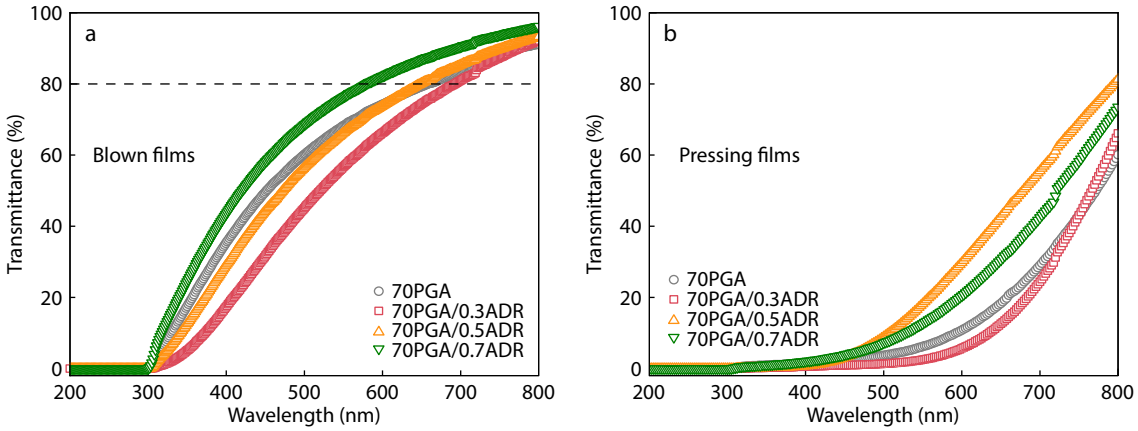

Fig. 8 UV-Vis spectra of the (a) blown films and (b) pressed films.

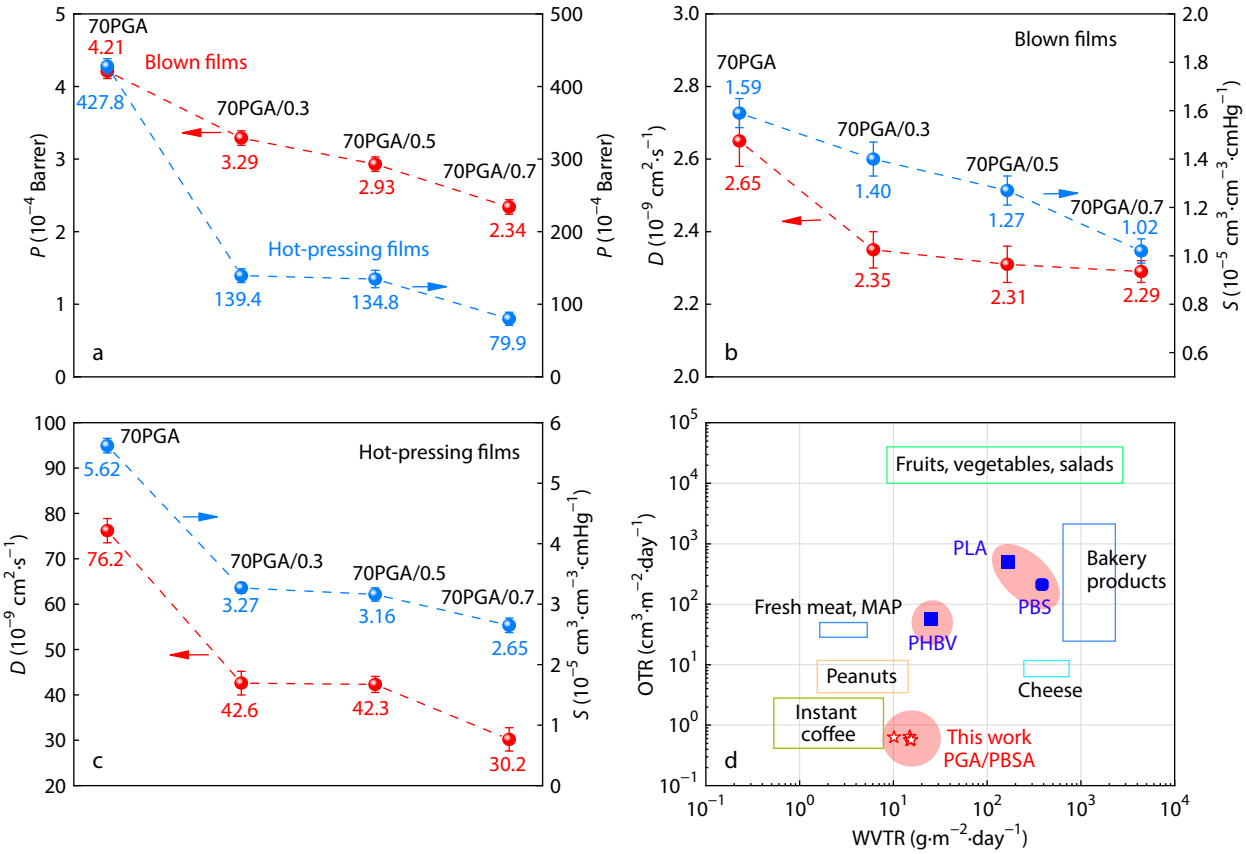

Fig. 9 Evaluation of the performance of the films to demonstrate their resistance to gas permeation. (a) Oxygen permeability of the blown and pressed films, and the diffusivity and solubility coefficient of the (b) blown films and (c) pressed films. (d) the optimum values of OTR and WVTR for different foods.

is 0.44 Barrer (Table S1 in ESI), which is a barrier performance that is three orders of magnitude lower than that of PGA. When gas molecules cross the interface between PGA and PBSA and enter the PBSA phase, the gas transmission significantly increases. However, the nanoscale PBSA in the blown films hinder the transmission of the gas molecules, and hence, the gas is more in contact with PGA than with PBSA during the permeation process. Therefore, the gas passes through the film faster as the size of PBSA increases.

Sato *et al.*[44] reported that the P_{O_2} of neat non-stretched PGA sheet is 7.5×10^{-4} Barrer. Compared to the pristine PGA sheet without oriented lamellae, the gas barrier properties of the PGA/PBSA (30 wt%) composite film did not decrease but increased. This is mainly due to the crystal orientation of PGA and the strong interfacial interaction between PGA and PBSA, both of which can increase the gas diffusion pathway and improve the barrier properties.

The permeation of the gas molecules through a polymeric film involves absorption, diffusion, and desorption.[45] Permeability is the product of the diffusion coefficient (*D*) and

solubility coefficient (S) ($P = D \times S$). As shown in Fig. S5 (in ESI), the typical oxygen permeation curves of the pristine PGA/PBSA blown and pressed films, showing the variations in the oxygen pressure in the downstream compartment as a function of time. The diffusion coefficient was calculated by the time-lag method. Figs. 9(b) and 9(c) illustrate the diffusion and solubility coefficients of the PGA/PBSA composite films to clarify the dependence of the barrier performance on the processing technology and ADR content. The solubility coefficient, S, is related to the free volume in the film structure, which is mainly a result of the adsorption of the gas molecules by the free volume formed by the interfacial defects (voids) and molecular chain spacing in the amorphous region. In this work, because the intermolecular interaction in PGA is very high, which is the main reason for the high density of PGA (1.51 g·cm^{-3}),[46] the adsorption of the molecules on its amorphous region is negligible. Therefore, mainly the defects at the interface contribute to S. Because the PBSA dimensions in the blown film are reduced to the nanoscale, the free volume on which the gas molecules could be adsorbed is decreased, leading to the reduction in S. As shown in Figs. 9(b) and 9(c), the S values of the composite films obtained by the two different processes are similar. The application of the elongation field leads to the orientation of the PGA crystals and the formation of fibrillar PBSA, which facilitates the diffusion of the gas molecules. Thus, it provides a more tortuous diffusion path, which is manifested in the drop of D.

The packaging films for certain food types require a good balance of oxygen and water barrier properties. Fig. 9(d) illustrates the optimum values of oxygen transmission rate (OTR) and water vapor transmission rate (WVTR) for different foods[47] and compares them with the results of this work (Table S1 in ESI). Fig. 9(d) indicates that the developed PGA/PBSA blown films satisfy the requirements for most instant foods such as coffee, peanuts, and fresh meat.

Tensile Properties of the Blown Films

The mechanical properties, especially tensile strength (σ), tearing strength, and elongation at break (ε), are also crucial for the films used in practical packaging applications. Fig. 10 and Table S2 (in ESI) show σ, ε, Young's modulus and tearing strength of neat PBSA and PGA/PBSA blown films with different content of ADR. Compared to 70PGA film without ADR, an improvement in the mechanical properties is observed after the addition of ADR. The σ, ε, Young's modulus and tearing strength of 70PGA/0.5ADR increased by approximately 32%, 26%, 64% and 48%, respectively, compared to those of the 70PGA film. The adhesion between the matrix and PBSA phase is improved after the addition of

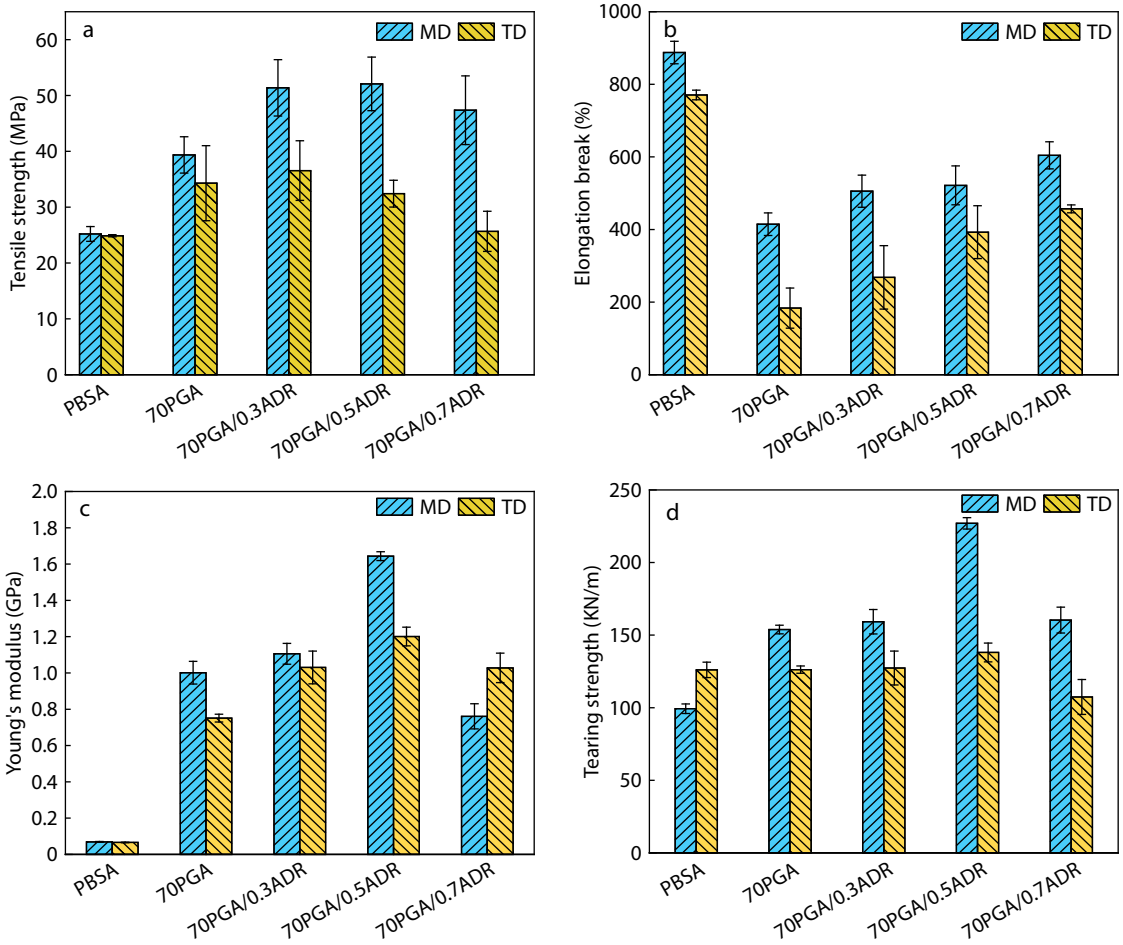

Fig. 10 Mechanical properties of the neat PBSA and 70PGA/ADR films: (a) tensile strength, (b) elongation at break, (c) Young's modulus, and (d) tearing strength.

Table 3 Comprehensive properties of the barrier films prepared in this work and in previous studies.

Samples	OTR ($cm^3 \cdot m^{-2} \cdot day^{-1}$)	O_2 Permeability (Barrer)	WVTR ($g \cdot m^{-2} \cdot day^{-1}$)	WVP (10^{-14} g·cm·$cm^{-2} \cdot s^{-1} \cdot Pa^{-1}$)	σ (MPa)	ε (%)	Refs.
70PGA/0.7ADR	0.57	2.34×10^{-4}	15.43	1.67	47.4	604.4	This work
60PGA/40/PBAT/1.5ADR	22.5	0.016	17.83	2.39	37.2	281.7	[21]
PBAT/PGA/ADR (65/35/0.9)		0.437		19.25	10.3	498.1	[46]
PBAT/PGA/GMA (80/20/2)	703	1.081	240		15.8	577.5	[48]
PBAT/PGA/GMA (80/20/2)-250 kGy	504	0.866	237		18.1	541.2	[48]
PBSA/PLA/C20A (10/90/4)		0.21		0.263	85	13.5	[49]
PBSA/PLA/thymol (30/70/6)				82.61	32.87	248.2	[50]
PBSA/PLA/ESA (80/20/3)	109.95	7.5	129.63	0.868	38.5	10.3	[51]

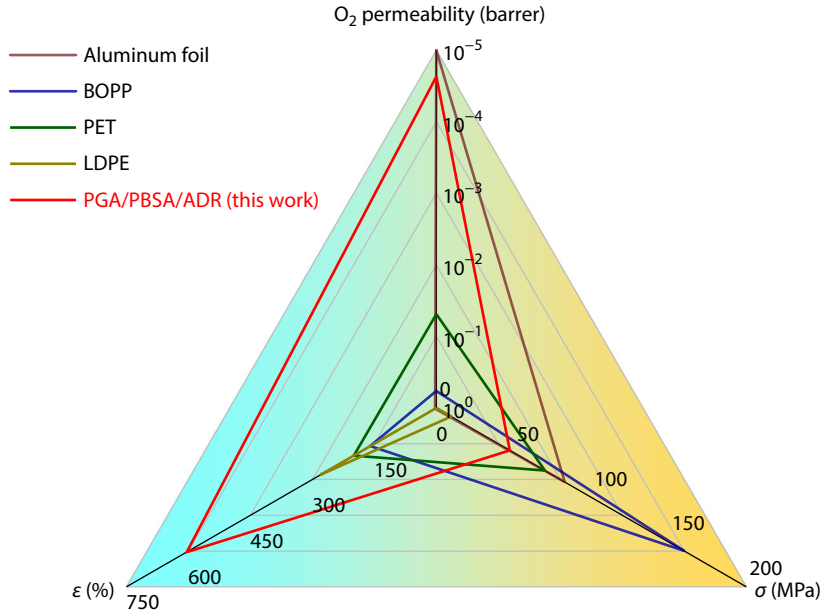

Fig. 11 Triangle performance to demonstrate the superiority of the 70PGA/0.7ADR blown film over other packaging films in terms of O_2 permeability, σ, and ε. The area size of each triangle represents the overall performance of the mateial.

the chain extender, and the significant orientation of the PBSA nanofibrils allow a suitable stress transfer between the ductile PBSA and PGA matrix, which improves the mechanical properties of the blend. On the other hand, except for ε, a reduction in the mechanical properties of the composite is observed when the ADR content reaches 0.7 phr (70PGA/0.7ADR). This can be attributed to the plasticizing and lubricating effects of the excess ADR, which remains unreacted. These effects increase ε and reduce σ, which is similar to their effects on the rheology properties (Fig. 3). Significant differences in the mechanical properties of the blown films are observed in the MD and TD. This behavior can be attributed to an imbalance in the orientation of the crystalline structure, which has been confirmed by the SAXS results and pole figures (Fig. 6).

Comprehensive Properties of the PGA/PBSA Blown Films

A comprehensive comparison of the performance (including oxygen and water vapor transport performance and mechanical properties) of the 70PGA/0.7ADR blown films of this work with those of other reported films containing PGA or PBSA/PLA films was conducted (Table 3). The 70PGA/0.7ADR film prepared in this work shows superior gas barrier performance, strength, and ductility. The P_{O2} of the 60PGA/40PBAT/ADR blown films developed in our previous work is approximately two orders of magnitude higher than 70PGA/ADR.[21] Moreover, the SEM images of the PBSA system show a longer and thinner microfibrillar structure than the PBAT system and a more blurred interface between the two phases. In 70PGA/ADR, the gas diffusion paths from the phase interface are reduced, indicating better barrier properties. In addition, a comprehensive comparison was conducted between the performance of the 70PGA/0.7ADR blown films developed here and that of commercial petroleum-based packing films such as LDPE, biaxial-oriented polypropylene (BOPP), and poly(ethylene terephthalate) (PET). As illustrated in Fig. 11, the 70PGA/0.7ADR blown film shows superior properties (outstanding mechanical properties and high oxygen barrier performance) to these of petroleum-based polymers.

CONCLUSIONS

PGA/PBSA films with outstanding gas barrier as well as mechanical and transparent properties have successfully been prepared *via* blown film extrusion based on the concept of *in situ* formation of nanofibrillar polymer-polymer composite. A

https://doi.org/10.1007/s10118-023-2972-9

unique hierarchical structure was assembled by PBSA nanofibrils, and interfacial oriented PGA crystals were obtained, which enhance the strength, ductility, and gas barrier properties of the PGA/PBSA blend film. 70PGA/0.7ADR exhibits a low oxygen permeability of 2.34×10^{-4} Barrer as well as significantly high ductility (604.4%), strength (47.4 MPa), and transparency, which are superior to those of petroleum-based polymers. Moreover, the 70PGA/0.7ADR blown films can satisfy the requirements for most instant foods such as coffee, peanuts, and fresh meat. The method used to prepare the films in this study is simple and highly promising. In addition, it utilizes less energy and employs a continuous and efficient industrial technique compared to other fabrication methods for packaging films. Thus, this is a sustainable method that uses renewable materials that can contribute to conserving the world's depleting natural resources.

Conflict of Interests

The authors declare no interest conflict.

Electronic Supplementary Information

Electronic supplementary information (ESI) is available free of charge in the online version of this article at http://doi.org/10.1007/s10118-023-2972-9.

ACKNOWLEDGMENTS

This study was financially supported by the National Key Research and Development Program of China (No. 2022YFB3704900), the National Natural Science Foundation of China (No. 52073004) and China National Tobacco Corporation Guizhou Company (No. 2023XM24).

REFERENCES

1 Hudson, M. J.; Aoyama, M.; Hoover, K. C.; Uchiyama, J. Prospects and challenges for an archaeology of global climate change. *Wiley Interdiscip. Rev. Clim. Change* **2012**, *3*, 313–328.
2 Zhao, X.; Ma, X.; Chen, B.; Shang, Y.; Song, M. Challenges toward carbon neutrality in China: strategies and countermeasures. *Resour. Conserv. Recycl.* **2022**, *176*, 105959.
3 Okura, M.; Takahashi, S.; Kobayashi, T.; Saijo, H.; Takahashi, T. In *Improvement of impact strength of polyglycolic acid for self-degradable tools for low-temperature wells*, SPE Middle East Unconventional Resources Conference and Exhibition, OnePetro: **2015**.
4 Yamane, K.; Sato, H.; Ichikawa, Y.; Sunagawa, K.; Shigaki, Y. Development of an industrial production technology for high-molecular-weight polyglycolic acid. *Polym. J.* **2014**, *46*, 769–775.
5 Valderrama, M. A. M.; van Putten, R. J.; Gruter, G. J. M. The potential of oxalic-and glycolic acid based polyesters (review). Towards CO_2 as a feedstock (Carbon Capture and Utilization-CCU). *Eur. Polym. J.* **2019**, *119*, 445–468.
6 Li, J. X.; Niu, D. Y.; Xu, P. W.; Sun, Z. Y.; Yang, W. J.; Ji, Y.; Ma, P. M. Tailoring the crystallization behavior and mechanical property of poly(glycolic acid) by self-nucleation. *Chinese J. Polym. Sci.* **2022**, *40*, 365–372.
7 Xu, P.; Tan, S.; Niu, D.; Yang, W.; Ma, P. Highly toughened sustainable green polyglycolic acid/polycaprolactone blends with balanced strength: morphology evolution, interfacial compatibilization, and mechanism. *ACS Appl. Polym. Mater.* **2022**, *4*, 5772–5780.
8 Samantaray, P. K.; Little, A.; Haddleton, D. M.; McNally, T.; Tan, B.; Sun, Z.; Huang, W.; Ji, Y.; Wan, C. Poly(glycolic acid) (PGA): a versatile building block expanding high performance and sustainable bioplastic applications. *Green Chem.* **2020**, *22*, 4055–4081.
9 Kuredux Polyglycolic Acid (PGA) Resin, A New Polymer Option. http://www.kureha.com/product-groups/pga.htm.
10 Shunsuke, A. Successively biaxially stretched polyglycolic acid film, process for producing the successively biaxially stretched polyglycolic acid film, and multilayered film. WO: **2010**.
11 Kawakami, Y.; Sato, N.; Hoshino, M.; Kouyama, T.; Shiiki, Z. Polyglycolic acid sheet and production process thereof. Google Patents: **1999**.
12 Lin, Y.; Bilotti, E.; Bastiaansen, C. W.; Peijs, T. Transparent semi-crystalline polymeric materials and their nanocomposites: a review. *Polym. Eng. Sci.* **2020**, *60*, 2351–2376.
13 Wang, R.; Sun, X.; Chen, L.; Liang, W. Morphological and mechanical properties of biodegradable poly(glycolic acid)/poly(butylene adipate-*co*-terephthalate) blends with *in situ* compatibilization. *RSC Adv.* **2021**, *11*, 1241–1249.
14 Niu, D.; Xu, P.; Sun, Z.; Yang, W.; Dong, W.; Ji, Y.; Liu, T.; Du, M.; Lemstra, P. J.; Ma, P. Superior toughened bio-compostable poly(glycolic acid)-based blends with enhanced melt strength *via* selective interfacial localization of *in-situ* grafted copolymers. *Polymer* **2021**, *235*, 124269.
15 Ellingford, C.; Samantaray, P. K.; Farris, S.; McNally, T.; Tan, B.; Sun, Z.; Huang, W.; Ji, Y.; Wan, C. Reactive extrusion of biodegradable PGA/PBAT blends to enhance flexibility and gas barrier properties. *J. Appl. Polym. Sci.* **2021**, *139*, 51617.
16 Magazzini, L.; Grilli, S.; Fenni, S. E.; Donetti, A.; Cavallo, D.; Monticelli, O. The blending of poly(glycolic acid) with polycaprolactone and poly(l-lactide): promising combinations. *Polymers* **2021**, *13*, 2780.
17 Wang, K.; Shen, J.; Ma, Z.; Zhang, Y.; Xu, N.; Pang, S. Preparation and properties of poly(ethylene glycol-*co*-cyclohexane-1,4-dimethanol terephthalate)/polyglycolic acid (PETG/PGA) blends. *Polymers* **2021**, *13*, 452.
18 Chang, L. F.; Zhou, Y. G.; Ning, Y.; Zou, J. Toughening effect of physically blended polyethylene oxide on polyglycolic acid. *J. Polym. Environ.* **2020**, *28*, 2125–2136.
19 Vartiainen, J.; Shen, Y.; Kaljunen, T.; Malm, T.; Vähä-Nissi, M.; Putkonen, M.; Harlin, A. Bio-based multilayer barrier films by extrusion, dispersion coating and atomic layer deposition. *J. Appl. Polym. Sci.* **2016**, *133*, 42260.
20 Samantaray, P. K.; Ellingford, C.; Farris, S.; Tan, B.; Sun, Z.; Mcnally, T.; Wan, C. Electron beam-mediated cross-linking of blown film-extruded biodegradable PGA/PBAT blends toward high toughness and low oxygen permeation. *ACS Sustainable Chem. Eng.* **2022**, *10*, 1267–1276.
21 Yang, F.; Zhang, C.; Ma, Z.; Weng, Y. *In situ* formation of microfibrillar PBAT in PGA films: an effective way to robust barrier and mechanical properties for fully biodegradable packaging films. *ACS Omega* **2022**, *7*, 21280–21290.
22 Zhou, S. Y.; Huang, H. D.; Ji, X.; Yan, D. X.; Zhong, G. J.; Hsiao, B. S.; Li, Z. M. Super-robust polylactide barrier films by building densely oriented lamellae incorporated with ductile *in situ* nanofibrils of poly(butylene adipate-*co*-terephthalate). *ACS Appl. Mater. Interfaces* **2016**, *8*, 8096–109.
23 Yousfi, M.; Dadouche, T.; Chomat, D.; Samuel, C.; Soulestin, J.; Lacrampe, M. F.; Krawczak, P. Development of nanofibrillar morphologies in poly(L-lactide)/poly (amide) blends: role of the

matrix elasticity and identification of the critical shear rate for the nodular/fibrillar transition. *RSC Adv.* **2018**, *8*, 22023–22041.
24 Wang, G.; Zhao, J.; Wang, G.; Zhao, H.; Lin, J.; Zhao, G.; Park, C. B. Strong and super thermally insulating *in situ* nanofibrillar PLA/PET composite foam fabricated by high-pressure microcellular injection molding. *Chem. Eng. J.* **2020**, *390*, 124520.
25 Chomat, D.; Soulestin, J.; Lacrampe, M. F.; Sclavons, M.; Krawczak, P. *In situ* fibrillation of polypropylene/polyamide 6 blends: Effect of organoclay addition. *J. Appl. Polym. Sci.* **2015**, *132*, 41680.
26 Ojijo, V.; Ray, S. S. Super toughened biodegradable polylactide blends with non-linear copolymer interfacial architecture obtained *via* facile *in-situ* reactive compatibilization. *Polymer* **2015**, *80*, 1–17.
27 Sun, Q.; Mekonnen, T.; Misra, M.; Mohanty, A. K. Novel biodegradable cast film from carbon dioxide based copolymer and poly(lactic acid). *J. Polym. Environ.* **2015**, *24*, 23–36.
28 Li, X.; Yan, X.; Yang, J.; Pan, H.; Gao, G.; Zhang, H.; Dong, L. Improvement of compatibility and mechanical properties of the poly(lactic acid)/poly(butylene adipate-*co*-terephthalate) blends and films by reactive extrusion with chain extender. *Polym. Eng. Sci.* **2018**, *58*, 1868–1878.
29 Messin, T.; Follain, N.; Guinault, A.; Sollogoub, C.; Gaucher, V.; Delpouve, N.; Marais, S. Structure and barrier properties of multinanolayered biodegradable PLA/PBSA films: confinement effect *via* forced assembly coextrusion. *ACS Appl. Mater. Interfaces* **2017**, *9*, 29101–29112.
30 Chiu, F. C.; Hsieh, Y. C.; Sung, Y. C.; Liang, N. Y. Poly(butylene succinate-*co*-adipate) green composites with enhanced rigidity: influences of dimension and surface modification of Kenaf fiber reinforcement. *Ind. Eng. Chem. Res.* **2015**, *54*, 12826–12835.
31 Jiang, G.; Yu, L. High strength and barrier properties of biodegradable PPC/PBSA blends prepared by reaction compatibilization for promising application in packaging. *Macromol. Mater. Eng.* **2021**, (306), 2000723.
32 Purahong, W.; Wahdan, S. F. M.; Heinz, D.; Jariyavidyanont, K.; Sungkapreecha, C.; Tanunchai, B.; Sansupa, C.; Sadubsarn, D.; Alaneed, R.; Heintz-Buschart, A.; Schadler, M.; Geissler, A.; Kressler, J.; Buscot, F. Back to the future: decomposability of a biobased and biodegradable plastic in field soil environments and its microbiome under ambient and future climates. *Environ. Sci. Technol.* **2021**, *55*, 12337–12351.
33 Yousfi, M.; Soulestin, J.; Marcille, S.; Lacrampe, M. F. *In-situ* nano-fibrillation of poly(butylene succinate-co-adipate) in isosorbide-based polycarbonate matrix. Relationship between rheological parameters and induced morphological and mechanical properties. *Polymer* **2021**, *217*, 123445.
34 Nakafuku, C.; Yoshimura, H. Melting parameters of poly(glycolic acid). *Polymer* **2004**, *45*, 3583–3585.
35 Xu, H. S.; Li, Z. M.; Pan, J. L.; Yang, M. B.; Huang, R. Morphology and rheological behaviors of polycarbonate/high density polyethylene *in situ* microfibrillar blends. *Macromol. Mater. Eng.* **2004**, *289*, 1087–1095.
36 Xia, X. C.; Yang, W.; He, S.; Xie, D. D.; Zhang, R. Y.; Tian, F.; Yang, M. B. Formation of various crystalline structures in a polypropylene/polycarbonate *in situ* microfibrillar blend during the melt second flow. *Phys. Chem. Chem. Phys.* **2016**, *18*, 14030–14039.
37 Evstatiev, M. Manufacturing and characterization of microfibrillar reinforced composites from polymer blends. *Polym. Compos.* **2005**, 149–167.
38 Gu, S. Y.; Zhang, K.; Ren, J.; Zhan, H. Melt rheology of polylactide/poly(butylene adipate-*co*-terephthalate) blends. *Carbohydr. Polym.* **2008**, *74*, 79–85.
39 Wang, R.; Sun, X.; Chen, L.; Liang, W. Morphological and mechanical properties of biodegradable poly(glycolic acid)/poly(butylene adipate-*co*-terephthalate) blends with *in situ* compatibilization. *RSC Adv.* **2021**, *11*, 1241–1249.
40 Pan, H.; Li, Z.; Yang, J.; Li, X.; Ai, X.; Hao, Y.; Zhang, H.; Dong, L. The effect of MDI on the structure and mechanical properties of poly(lactic acid) and poly(butylene adipate-*co*-butylene terephthalate) blends. *RSC Adv.* **2018**, *8*, 4610–4623.
41 Murcia Valderrama, M. A.; van Putten, R. J.; Gruter, G. M. PLGA barrier materials from CO_2. The influence of lactide co-monomer on glycolic acid polyesters. *ACS Appl. Polym. Mater.* **2020**, *2*, 2706–2718.
42 Lee, S.; Hongo, C.; Nishino, T. Crystal modulus of poly(glycolic acid) and its temperature dependence. *Macromolecules* **2017**, *50*, 5074–5079.
43 Montes de Oca, H.; Ward, I. M. Structure and mechanical properties of PGA crystals and fibres. *Polymer* **2006**, *47*, 7070–7077.
44 Sato, H.; Yamane, K.; Hokari, Y.; Kobayashi, F.; Kuruhara, N.; Ichikawa, Y.; Oishi, Y. Preparation and characterization of poly(ethylene terephtalate)/polyglycolic acid blends by simple extruding process. *KOBUNSHI RONBUNSHU* **2011**, *68*, 719–730.
45 Robeson, L. M. The upper bound revisited. *J. Membr. Sci.* **2008**, *320*, 390–400.
46 Shen, J.; Wang, K.; Ma, Z.; Xu, N.; Pang, S.; Pan, L. Biodegradable blends of poly(butylene adipate-*co*-terephthalate) and polyglycolic acid with enhanced mechanical, rheological and barrier performances. *J. Appl. Polym. Sci.* **2021**, *138*, e51285.
47 Wang, J.; Gardner, D. J.; Stark, N. M.; Bousfield, D. W.; Tajvidi, M.; Cai, Z. Moisture and oxygen barrier properties of cellulose nanomaterial-based films. *ACS Sustain. Chem. Eng.* **2018**, *6*, 49–70.
48 Samantaray, P. K.; Ellingford, C.; Farris, S.; O'Sullivan, D.; Tan, B.; Sun, Z.; McNally, T.; Wan, C. Electron beam-mediated cross-linking of blown film-extruded biodegradable PGA/PBAT blends toward high toughness and low oxygen permeation. *ACS Sustain. Chem. Eng.* **2022**, *10*, 1267–1276.
49 Ojijo, V.; Sinha Ray, S.; Sadiku, R. Concurrent enhancement of multiple properties in reactively processed nanocomposites of polylactide/poly[(butylene succinate)-*co*-adipate] blend and organoclay. *Macromol. Mater. Eng.* **2014**, *299*, 596–608.
50 Suwanamornlert, P.; Kerddonfag, N.; Sane, A.; Chinsirikul, W.; Zhou, W.; Chonhenchob, V. Poly(lactic acid)/poly(butylene-succinate-*co*-adipate) (PLA/PBSA) blend films containing thymol as alternative to synthetic preservatives for active packaging of bread. *Food Packag. Shelf Life* **2020**, *25*, 100515.
51 Palai, B.; Mohanty, S.; Nayak, S. K. Synergistic effect of polylactic acid (PLA) and poly(butylene succinate-*co*-adipate) (PBSA) based sustainable, reactive, super toughened eco-composite blown films for flexible packaging applications. *Polym. Test.* **2020**, *83*, 106130.

https://doi.org/10.1007/s10118-023-2972-9